



ELSEVIER

Contents lists available at ScienceDirect

Control Engineering Practice

journal homepage: www.elsevier.com/locate/conengprac

Robust anti-sliding control of autonomous vehicles in presence of lateral disturbances [☆]

Hao Fang ^{a,*}, Lihua Dou ^a, Jie Chen ^a, Roland Lenain ^b, Benoit Thuilot ^b, Philippe Martinet ^b

^a Key Laboratory of Complex System Intelligent Control and Decision, Beijing Institute of Technology, Beijing 100081, China

^b LASMEA, 24, av. des Landais, 63177 Aubiere Cedex, France

ARTICLE INFO

Article history:

Received 25 December 2009

Accepted 31 January 2011

Available online 21 February 2011

Keywords:

Anti-sliding control
Lateral disturbances
Chained system theory
Adaptive observer
Autonomous vehicles

ABSTRACT

Path following control problem of autonomous vehicles is investigated, concerning both unmeasurable sliding effects and lateral disturbances which lead to some difficulties in designing autonomous control under complex environment. To deal with the sliding effects, sideslip angles are modeled and reconstructed by estimating the tire cornering stiffness, which plays important role in analyzing the sliding effects. To this end, a Luenberger-type observer is designed, which is able to identify the tire cornering stiffness adaptively even in presence of time-varying lateral disturbances. Furthermore, to guarantee high-precision guidance, a sliding mode controller is designed based on chained system theory, and this controller is shown to be robust to both the lateral disturbances and the inaccuracy of the sliding reconstruction. Simulations illustrate that the proposed methods can reconstruct the sliding angles and provide high-accuracy anti-sliding control even in presence of the time-varying lateral disturbances.

© 2011 Elsevier Ltd. All rights reserved.

1. Introduction

Automatic steering control of intelligent vehicles has been studied actively. Considerable work has been carried out with the assumption of the pure rolling condition which is not true especially when the ground is wet and slippery. Stability and controllability of the autonomous vehicle systems may be violated because of unexpected sliding effects.

Several solutions have already been proposed to deal with sliding. Ackermann (1997) prevented cars from skidding by robust decoupling of car steering dynamics which was achieved by feedback of the integrated yaw rate into front wheel steering. Motte and Campion (2000) coped with the control of WMR (Wheeled Mobile Robot) dissatisfying the ideal kinematic constraints by using slow manifold methods, but the parameters characterizing the sliding effects were assumed to be exactly known. In Leroquais and D'Andrea-Novel (1997) a controller was designed based on the averaged model allowing tracking errors to converge to a limit cycle near the origin. In D'Andrea-Novel, Campion, and Bastin (1995) a general singular perturbation formulation was developed which led to robust results for linearizing feedback laws ensuring trajectory tracking. However, the schemes of Leroquais

and D'Andrea-Novel (1997) and D'Andrea-Novel et al. (1995) only took into account sufficiently small sliding effects. In Zhang, Chung, and Velinsky (2003) and Fang, Lenain, Thuilot, and Martinet (2004) Variable Structure Control (VSC) was used to eliminate harmful sliding effects when the bounds of the sliding effects had been known. The trajectory tracking problem of mobile robots in presence of sliding was solved by using discrete-time sliding mode control, but the controllers of Zhang et al. (2003), Fang et al. (2004) and Corradini and Orlando (2002) counteracted sliding effects **only** relying on high-gain controllers, without estimating and compensating sliding effects. Moreover, a robust adaptive controller was designed in Fang, Lenain, Thuilot, and Martinet (2005a) which compensated sliding effects by parameter adaptation and VSC. Fang, Lenain, Thuilot, and Martinet (2005b), Fang, Fan, Thuilot, and Martinet (2006), Wang and Low (2007), Low and Wang (2008) designed longitudinal and lateral anti-sliding controllers with backstepping methods for farm vehicles.

Since the tire cornering stiffness is one of the most important parameters for the lateral stability and handling characteristics of vehicles, estimation of the cornering stiffness plays a key role in sliding estimation and compensation. In Sierra, Tseng, Jain, and Peng (2006) the cornering stiffness was estimated in both time-domain and frequency-domain based on the vehicle bicycle model and common lateral/yaw measurements. In Hahn, Rajamani, and Alexander (2002) a new tire-road friction coefficient estimation algorithm was developed based on measurements related to the lateral dynamics of the vehicle. A differential

[☆] This work was supported by NSFC 60805035/F0306, 60925011.

* Corresponding author. Tel.: +86 10 68918976.

E-mail address: fangh@bit.edu.cn (H. Fang).

global positioning system (DGPS) and a gyroscope were used to identify the tire-road friction coefficient and cornering stiffness parameters. A two-block estimation process was developed by Baffet, Charara, and Lechner (2009). The first block contained a sliding mode observer to calculate the tire-road forces. The second block used an extended Kalman filter to estimate the sideslip angles and cornering stiffness. The estimation process based on the two blocks in series gave good estimates of the cornering stiffness.

In recent years, another framework of anti-sliding control relying on observer theories becomes more and more active. In Lenain, Thuilot, Cariou, and Martinet (2006a) and Lenain, Thuilot, Cariou, and Martinet (2006b), kinematic-based observers were designed with the concept of classical feedback control theories to estimate the sliding effects. In Hiraoka, Kumamoto, Nishihara, and Tenmoku (2001) an adaptive observer was developed to estimate the sideslip angles, but both the front/rear-side-acceleration and the yaw rate had to be measured. To estimate sliding perturbations, the RTK-GPS measurements were fused with other high-update rate navigation sensors, for example, the combination of GPS and inertial sensors were utilized to estimate sideslip angles for automobile stability control based on Kalman Filter (Low & Wang, 2007; Bevy, Gerdes, Wilson, & Zhang, 2000; Bevy, Sheridan, & Gerdes, 2000; Bevy, 2004).

From the above literature, it is quite evident that (robust) observer-based approaches provide an effective solution to identify the tire cornering stiffness under complex working conditions with output noises, parameter variations as well as sustained disturbances. On the other hand, for both technical and economical reasons, it is not allowed to install two GPS antennas or two side-accelerometers in a standard car. So in this paper only one GPS is applied to locate vehicle position. And only one side-acceleration and yaw rate of the vehicles are measured. Because it is difficult to identify time-varying variables (e.g., time-varying sliding angles) for a nonlinear system, the cornering stiffness which is only relevant to tire-ground contact characteristics is identified in presence of lateral disturbances by using a robust adaptive Luenberger observer. Furthermore a sliding mode controller is designed based on chained system theory to cope with inaccuracy of sliding angle reconstruction, leading to satisfactory results of anti-sliding control. This paper is organized as follows. In Section 2 the path following problem is described and a kinematic model considering sliding is constructed. In Section 3 the sliding angles are reconstructed through identifying the cornering stiffness. In Section 4 a robust anti-sliding controller is designed. In Section 5 some comparative results are presented to validate the proposed control laws.

2. Kinematic model for path following control

2.1. Notation and problem description

In this paper the vehicle model is based on an Ackermann model. The description of the vehicle motion is made with respect to the path to be followed (M, η_t, η_n). Variables appearing in the kinematic model are denoted as follows: (see Fig. 1)

- C is the path to be followed.
- O is the center of the vehicle virtual rear wheel.
- M is the orthogonal projection of O on path C .
- η_t is the tangent vector at M .
- η_n is the normal vector at M .
- y is the lateral deviation between O and M .
- s is the curvilinear coordinates (arc-length) of point M along the path from an initial position.
- $c(s)$ is the curvature of the path at point M .

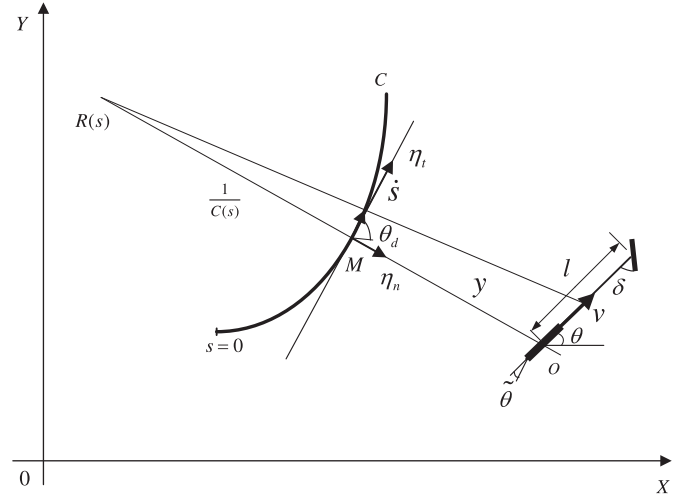


Fig. 1. Notation and path frame description.

- $\theta_d(s)$ is the orientation of the tangent to the path at point M with respect to the inertia frame.
- θ is the orientation of the vehicle centerline with respect to the inertia frame.
- $\tilde{\theta} = \theta - \theta_d$ is the orientation error.
- l is the vehicle wheelbase.
- v is the vehicle longitudinal linear velocity.
- δ is the steering angle of the virtual front wheel

So the vehicle motion can be described by $(y, s, \tilde{\theta})$. In this paper for the autonomous vehicles deployed in complex and uncertain environments, an anti-sliding control law

$$\delta = K(s, y, \tilde{\theta}, v) \tag{1}$$

is to be designed to guarantee $y(t)$ and $\tilde{\theta}(t)$ ultimately bounded in presence of sliding and lateral disturbances. For simplicity, in the following text the dependency with time (t) will be omitted.

2.2. Kinematic model

When autonomous vehicles move without sliding, the ideal kinematic model of the vehicles is (see Thuilot, Cariou, Martinet, & Berducat, 2002 for details).

$$\begin{cases} \dot{s} = \frac{v \cos \tilde{\theta}}{1 - c(s)y} \\ \dot{y} = v \sin \tilde{\theta} \\ \dot{\tilde{\theta}} = v \left(\frac{\tan \delta}{l} - \frac{c(s) \cos \tilde{\theta}}{1 - c(s)y} \right) \end{cases} \tag{2}$$

But when the autonomous vehicles move on a steep slope or on a slippery ground, lateral tire forces may change prominently and tire sliding will occur inevitably. Therefore, (2) is no longer valid in the case of sliding. Violation of the pure rolling constraints can be described by introducing two tire sliding angles, which are the rear sliding angle α_r and the front sliding angle (also called Steering Angle Bias) δ_b (Fig. 2).

$$\delta_b = \delta - \frac{l_f \gamma + v \tan \beta}{v} \tag{3}$$

$$\alpha_r = \frac{-l_r \gamma + v \tan \beta}{v} \tag{4}$$

where β is the sideslip angle of the vehicle and γ is the yaw rate at the mass center, l_f (l_r) is the distance between the front (rear) wheel and the mass center.

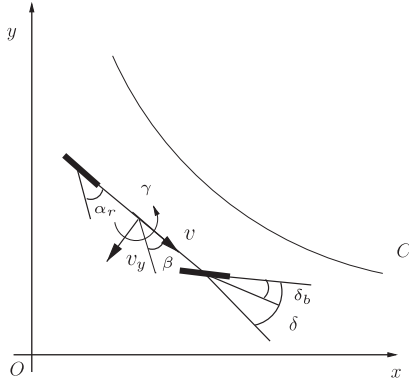


Fig. 2. Notations of sliding effects.

Similar methods lead to a tire-oriented kinematic model (Lenain et al., 2006a)

$$\begin{cases} \dot{s} = \frac{v \cos(\tilde{\theta} + \alpha_r)}{1 - c(s)y} \\ \dot{y} = v \sin(\tilde{\theta} + \alpha_r) \\ \dot{\tilde{\theta}} = v \left[\cos \alpha_r \frac{\tan(\delta + \delta_b) - \tan \alpha_r}{l} - \frac{c(s) \cos(\tilde{\theta} + \alpha_r)}{1 - c(s)y} \right] \end{cases} \quad (5)$$

If the tire sliding angles α_r, δ_b have been known, the negative sliding effects can be exactly compensated based on (5). So reconstruction of the tire sliding angles is the first object to be attained.

3. Sliding angle reconstruction

3.1. 2DOF lateral vehicle dynamics

For all-terrain-vehicles (ATVs), lateral disturbances which are possibly caused by bumps and ruts in the road surface or tire pressure loss are the most common type of external disturbances. Therefore, a 2DOF vehicle dynamic model with the lateral disturbances is adopted as follows (Abe, 1992; Hiraoka, Kumamoto, & Nishihara, 2004).

$$\dot{x} = Ax + Bu + \Psi \zeta \quad (6)$$

where

$$x = [v_y \quad \gamma]^T \quad (7)$$

$$A = \begin{bmatrix} -\frac{p_1}{mv} & -v + \frac{p_2}{mv} \\ \frac{p_2}{I_z v} & \frac{p_3}{I_z v} \end{bmatrix} \quad (8)$$

$$B = \begin{bmatrix} \frac{k_f}{m} & \frac{k_f l_f}{I_z} \end{bmatrix}^T \quad (9)$$

$$\Psi = \begin{bmatrix} \frac{1}{m} & -\frac{l_d}{I_z} \end{bmatrix}^T \quad (10)$$

$$I_z = m l_r l_f \quad (11)$$

$$p_1 = k_f + k_r \quad (12)$$

$$p_2 = k_r l_r - k_f l_f \quad (13)$$

$$p_3 = k_f l_f^2 + k_r l_r^2 \quad (14)$$

where u is the vector of the steering law δ . I_z is the inertia moment around z -axis. v_y and γ are the lateral velocity and the yaw rate at the mass center, respectively, ζ indicates the time-varying lateral disturbance. l_d is the distance between the disturbance location and the mass center. k_f (k_r) represents the cornering stiffness of the front (rear) tire which is approximately constant or varies slowly.

Assuming the vehicle moves with a constant forward velocity and differentiating (6) yield

$$\dot{X} = AX + BU + \Psi \dot{\zeta} \quad (15)$$

where

$$X = \dot{x} = \begin{bmatrix} \dot{v}_y \\ \dot{\gamma} \end{bmatrix} = \begin{bmatrix} a_g - v\gamma \\ \dot{\gamma} \end{bmatrix} \quad (16)$$

$$U = \dot{u} \quad (17)$$

and a_g is the body side-acceleration.

3.2. State equation of sideslip angle

Derived from the lateral kinematic relationship

$$\dot{v}_y = a_g - v\gamma \quad (18)$$

a_g can be written as

$$a_g = [v \quad 0 \quad v] \begin{bmatrix} \dot{\beta} \\ \dot{\gamma} \\ \dot{\theta} \end{bmatrix} = T \dot{\tilde{x}} \quad (19)$$

Furthermore the dynamic equation describing the relationship between the sideslip angle β and the yaw rate γ is considered (Hiraoka et al., 2004)

$$\dot{\tilde{x}} = A_1 \tilde{x} + B_1 u + \Psi_1 \zeta \quad (20)$$

where

$$\tilde{x} = [\beta \quad \gamma \quad \theta]^T \quad (21)$$

$$A_1 = \begin{bmatrix} -\frac{p_1}{mv} & -1 + \frac{p_2}{mv^2} & 0 \\ \frac{p_2}{I_z} & -\frac{p_3}{I_z v} & 0 \\ 0 & 1 & 0 \end{bmatrix} \quad (22)$$

$$B_1 = \begin{bmatrix} \frac{k_f}{mv} & \frac{k_f l_f}{I_z} & 0 \end{bmatrix}^T \quad (23)$$

$$\Psi_1 = \begin{bmatrix} \frac{1}{mv} & -\frac{l_d}{I_z} & 0 \end{bmatrix}^T \quad (24)$$

Substituting (20) into (19) can lead to

$$a_g = TA_1 \tilde{x} + TB_1 u + T\Psi_1 \zeta \quad (25)$$

Hence the expression of the sideslip angle β can be obtained by solving the above equation.

$$\beta = \frac{k_f}{k_f + k_r} u - \frac{k_f l_f - k_r l_r}{v(k_f + k_r)} \gamma - \frac{m}{k_f + k_r} a_g + \frac{1}{k_f + k_r} \zeta \quad (26)$$

Remark that the side-acceleration a_g is measurable and γ can be obtained with a yaw gyroscope, so as long as the cornering stiffness k_f, k_r has been identified, the unmeasurable sideslip angle β can be reconstructed by (27)

$$\hat{\beta}_r = \frac{\hat{k}_f}{\hat{k}_f + \hat{k}_r} u - \frac{\hat{k}_f l_f - \hat{k}_r l_r}{v(\hat{k}_f + \hat{k}_r)} \gamma - \frac{m}{\hat{k}_f + \hat{k}_r} a_g + \frac{1}{\hat{k}_f + \hat{k}_r} \zeta = \hat{\beta} + \frac{1}{\hat{k}_f + \hat{k}_r} \zeta \quad (27)$$

where $\hat{k}_f(\hat{k}_r)$ is the identification result of $k_f(k_r)$. Therefore, the problem of how to identify k_f, k_r becomes a key issue for reconstructing the sideslip angle β . But due to inaccuracy of \hat{k}_f, \hat{k}_r and uncertainty of ξ , the reconstructed sideslip angle $\hat{\beta}$ is subjected to a certain amount of errors.

After the sideslip angle β is reconstructed, it is quite straightforward to acquire the two tire sliding angles just by utilizing (3) and (4).

3.3. Identifying cornering stiffness by using robust adaptive observer

Due to the existence of ξ in (15), the following linear robust Luenberger observer is applied to identify k_f, k_r (Stephant, Charara, & Meizel, 2004)

$$\begin{cases} \dot{X} = AX + BU + \Psi \xi \\ \dot{\hat{X}} = \hat{A}\hat{X} + \hat{B}U + K(X - \hat{X}) + \Lambda \text{sign}(X - \hat{X}) \end{cases} \quad (28)$$

where \hat{A}, \hat{B} are the matrices containing the identification results \hat{k}_f, \hat{k}_r of the unknown cornering stiffness, which is assumed nearly constant.

$$\hat{A} = \begin{bmatrix} \frac{\hat{k}_f + \hat{k}_r}{mv} & -v + \frac{\hat{k}_r l_r - \hat{k}_f l_f}{mv} \\ \frac{\hat{k}_r l_r - \hat{k}_f l_f}{I_z v} & \frac{\hat{k}_f l_f^2 + \hat{k}_r l_r^2}{I_z v} \end{bmatrix} \quad (29)$$

$$\hat{B} = \begin{bmatrix} \hat{k}_f & \hat{k}_f l_f \\ m & I_z \end{bmatrix}^T \quad (30)$$

$K = \text{diag}(k_1, k_2)$ is a matrix such that $(A - K)$ is Hurwitz. \hat{X} is the estimated value. $\Lambda = \text{diag}(\lambda_1, \lambda_2)$ is the gain of the signum function.

Define the error of the state estimation as $e = \hat{X} - X$. The following equation holds by considering (28)

$$\dot{e} = A_e e + \tilde{W} \phi - \Psi \xi - \Lambda \text{sign}(e) \quad (31)$$

where

$$A_e = A - K \quad (32)$$

$$\tilde{W} = [W_1 \hat{X} + W_2 \dot{u} \quad W_3 \hat{X}] \quad (33)$$

$$\phi = \begin{bmatrix} \hat{k}_f - k_f \\ \hat{k}_r - k_r \end{bmatrix} \quad (34)$$

And in \tilde{W}

$$W_1 = \begin{bmatrix} \frac{1}{mv} & \frac{l_f}{mv} \\ \frac{l_f}{I_z v} & \frac{l_f^2}{I_z v} \end{bmatrix} \quad (35)$$

$$W_2 = \begin{bmatrix} \frac{1}{m} & \frac{l_f}{I_z} \end{bmatrix}^T \quad (36)$$

$$W_3 = \begin{bmatrix} \frac{1}{mv} & \frac{l_r}{mv} \\ \frac{l_r}{I_z v} & \frac{l_r^2}{I_z v} \end{bmatrix} \quad (37)$$

The adaptive learning rules for \hat{k}_f, \hat{k}_r may be obtained by using Lyapunov stability theory. The Lyapunov function is defined as

$$V = e^T P_0 e + \phi^T Q_0 \phi \quad (38)$$

where $P_0 = \text{diag}(p_a, p_\gamma)$ and Q_0 are the symmetric positive definite matrices and P_0 satisfies $A_e^T P_0 + P_0 A_e = -Q_1 < 0$, then the time

derivative of V is

$$\begin{aligned} \dot{V} &= -e^T Q_1 e + 2\phi^T (\tilde{W}^T P_0 e + Q_0 \dot{\phi}) - 2\xi \Psi^T P_0 e - 2[1 \ 1] \Lambda P_0 |e| \\ &< -e^T Q_1 e + 2\phi^T (\tilde{W}^T P_0 e + Q_0 \dot{\phi}) + 2(|\xi \Psi^T| - [1 \ 1] \Lambda) P_0 |e| \end{aligned} \quad (39)$$

where $\Lambda = \text{diag}(\lambda_1, \lambda_2)$ is the gain to be designed. Assume estimation of the maximum disturbance derivative $\dot{\xi}$ is available and let

$$\dot{\phi} = \begin{bmatrix} \dot{\hat{k}}_f \\ \dot{\hat{k}}_r \end{bmatrix} = -Q_0^{-1} \tilde{W}^T P_0 e \quad (40)$$

$$\lambda_i > |\xi \Psi^T|_{1 \times i} \quad (41)$$

It can be obtained that

$$\dot{V} < -e^T Q_1 e \quad (42)$$

which guarantees the convergence of the linear Luenberger observer.

From (42) it is concluded that $e \rightarrow 0, \dot{e} \rightarrow 0$. Therefore, when \tilde{W} is full rank (which is easy to be carried out due to the definition of (33)), the identification error ϕ of the cornering stiffness is bounded (depending on the values of ξ). It is also noted that if the lateral disturbance is constant (or changes very slowly), the identified values of the cornering stiffness will converge to its real values.

Once the cornering stiffness has been identified, the vehicle sideslip angle β can be estimated and the tire sliding angles δ_b and α_r can be reconstructed. But actually due to inherent difficulties in modeling the lateral disturbances in Eq. (6) and the slowly-varying cornering stiffness, the reconstructed δ_b, α_r are not identical to their real values. Therefore, a robust controller is to be proposed to improve robustness against the reconstruction errors.

4. Robust anti-sliding controller design based on chained system theory

4.1. Chained system properties

As presented in Thuilot et al. (2002), a path following controller has been designed by converting the model (2) into a chained system which allows using linear system theories to design nonlinear controllers without any approximation while still relying on the actual nonlinear system model (see Samson, 1995). For a 3-D nonlinear system with two control inputs, the general chained system is written as

$$\text{derivation w.r.t } t \begin{cases} \dot{a}_1 = m_1 \\ \dot{a}_2 = a_3 m_1 \\ \dot{a}_3 = m_2 \end{cases} \quad (43)$$

where $A = [a_1, a_2, a_3]$ and $M = [m_1, m_2]$ are, respectively, the states and control inputs of the chained system. The general chained system can be converted into a single-input linear system by replacing the time derivative with a derivation with respect to the state variable a_1 . Using the notation

$$\frac{d}{da_1} a_i = a'_i \quad \text{and} \quad m_3 = \frac{m_2}{m_1} \quad (44)$$

the general 3-D chained system is changed into

$$\text{derivation w.r.t } \mathbf{a}_1 \begin{cases} a'_1 = 1 \\ a'_2 = a_3 \\ a'_3 = m_3 \end{cases} \quad (45)$$

where m_3 is the virtual control input.

Usually the virtual control input m_3 is designed to be a PD-type controller

$$m_3 = -K_d a_3 - K_p a_2 \quad (K_p, K_d) \in R^{+2} \quad (46)$$

which leads to

$$a''_2 + K_d a'_2 + K_p a_2 = 0 \quad (47)$$

It is easy to prove that the states a_2 and a_3 can converge to zero asymptotically by choosing appropriate K_d, K_p .

4.2. Robust anti-sliding controller design

When the lateral disturbances have to be considered, the reconstructed $\hat{\delta}_b, \hat{\alpha}_r$ suffer from a certain amount of the reconstruction errors. To overcome this problem, robust anti-sliding controllers which are robust to both the uncertain lateral disturbances and the reconstruction errors must be designed.

In this paper only the vehicle's lateral motion is considered and it is assumed that the tire sliding introduces weak effects on the longitudinal motion. Substituting the reconstructed tire sliding angles $\hat{\delta}_b, \hat{\alpha}_r$ into (5) and ignoring the inaccuracy of $\hat{\alpha}_r$ on the longitudinal direction, it is obtained that

$$\begin{cases} \dot{s} = \frac{v \cos(\tilde{\theta} + \hat{\alpha}_r)}{1 - c(s)y} \\ \dot{y} = v \sin(\tilde{\theta} + \hat{\alpha}_r) + \varepsilon_1 \\ \dot{\theta} = v \left[\cos \hat{\alpha}_r \frac{\tan(\delta + \hat{\delta}_b) - \tan \hat{\alpha}_r}{l} - \frac{c(s) \cos(\tilde{\theta} + \hat{\alpha}_r)}{1 - c(s)y} \right] + \varepsilon_2 \end{cases} \quad (48)$$

where ε_i is the vector indicating all the unformulated perturbation effects which are synthetically caused by both the inaccuracy of $\hat{\delta}_b, \hat{\alpha}_r$ and the lateral disturbances on the lateral and orientation kinematics.

Considering the kinematic model (48), via state transformation as following (Samson, 1995)

$$(a_1, a_2, a_3) = (s, y, (1 - c(s)y) \tan(\tilde{\theta} + \hat{\alpha}_r)) \quad (49)$$

a perturbed chained system can be obtained

$$\text{derivation w.r.t } t \begin{cases} \dot{a}_1 = \frac{v \cos(\tilde{\theta} + \hat{\alpha}_r)}{1 - yc(s)} = m_1 \\ \dot{a}_2 = v \sin(\tilde{\theta} + \hat{\alpha}_r) + \varepsilon_1 = a_3 m_1 + \varepsilon_1 \\ \dot{a}_3 = \frac{d}{dt} ((1 - yc(s)) \tan(\tilde{\theta} + \hat{\alpha}_r)) = m_2 + \eta \end{cases} \quad (50)$$

where

$$\begin{aligned} m_2 = & -vc(s) \sin(\tilde{\theta} + \hat{\alpha}_r) \tan(\tilde{\theta} + \hat{\alpha}_r) - v \frac{dc(s)}{ds} \frac{\cos(\tilde{\theta} + \hat{\alpha}_r)}{1 - yc(s)} \tan(\tilde{\theta} + \hat{\alpha}_r) y \\ & + v \frac{1 - yc(s)}{\cos^2(\tilde{\theta} + \hat{\alpha}_r)} \left(\cos(\hat{\alpha}_r) \frac{\tan(\delta + \hat{\delta}_b) - \tan \hat{\alpha}_r}{l} - c(s) \frac{\cos(\tilde{\theta} + \hat{\alpha}_r)}{1 - yc(s)} \right) \\ & + \frac{1 - yc(s)}{\cos^2(\tilde{\theta} + \hat{\alpha}_r)} \frac{d}{dt} \hat{\alpha}_r \end{aligned} \quad (51)$$

$$\eta = \frac{(1 - yc(s)) \varepsilon_2}{\cos^2(\tilde{\theta} + \hat{\alpha}_r)} - c(s) \varepsilon_1 \tan(\tilde{\theta} + \hat{\alpha}_r) \quad (52)$$

Note that in (50) ε_1 and η play a role as two additional perturbations to the ideal chained system, so (50) can also be converted into a perturbed single-input linear system

$$\text{derivation w.r.t } \mathbf{a}_1 \begin{cases} a'_1 = 1 \\ a'_2 = a_3 + \frac{\varepsilon_1}{m_1} \\ a'_3 = \frac{m_2}{m_1} + \frac{\eta}{m_1} = u_v + \frac{\eta}{m_1} \end{cases} \quad (53)$$

where $u_v = m_2/m_1$ is the virtual control input of the perturbed single-input system (53). Because the single-input model (53)

contains uncertain disturbances which are assumed to be bounded, theories of sliding mode control are applied to design a robust controller which may guarantee the system states converge to a neighborhood near the origin.

Concerning the states a_2, a_3 for the path following control, the manifold of the sliding mode control is defined as

$$z = A_s a_2 + a_3 \quad (54)$$

where A_s defines the slope of the manifold. One condition that guarantees the system states reach the manifold $z=0$ in finite time and remain in this mode is $z\dot{z} < 0$.

Theorem 1. Define a strictly increasing function

$$s(t) = \int_0^t v^+(\tau) d\tau \quad (55)$$

where v^+ is positive definite. Use the notation that $(\diamond)' = d \diamond / ds$. If the sign of $v^+(\tau)$ is kept positive, then the condition $z\dot{z} < 0$ is equivalent to the reaching condition $z\dot{z} < 0$.

Theorem 2. Considering the system (50) where $(a_1, a_2, a_3) = (s, y, (1 - c(s)y) \tan(\tilde{\theta} + \hat{\alpha}_r))$, we define

$$z = A_s a_2 + a_3 = A_s y + (1 - yc(s)) \tan(\tilde{\theta} + \hat{\alpha}_r) \quad (56)$$

The achievement of reaching the manifold (56) and remaining on it can be guaranteed by the control law

$$u_v = -K_s z - A_s a_3 - \rho \text{sign}(z) \quad (57)$$

where

$$\rho \geq |z| = \left| \frac{A_s \varepsilon_1 + \eta}{m_1} \right| \quad (58)$$

Please refer to Fang et al. (2004) for more details.

Since the sliding effects have been largely compensated by directly integrating the reconstructed sliding angles into the controller (see definition of u_v), the gain of the robust control term $\rho \text{sign}(z)$ can be set smaller than that of the robust controllers which solely rely on high-gain robust terms to counteract both the sliding effects and uncertain disturbances.

On the manifold (56), the following holds

$$z = A_s a_2 + a_3 = 0 \quad (59)$$

which leads to

$$a'_2 = -A_s a_2 + \frac{\varepsilon_1}{m_1} = -A_s a_2 + \varpi \quad (60)$$

The stability of system (60) has been analyzed in Jiang and Hill (1999) in detail. From (60) a_2 can be expressed as

$$a_2 = e^{-A_s s} a_2(0) + \varpi^* = a_2(0) e^{-A_s \int_0^s v^+(\tau) d\tau} + \varpi^* \quad (61)$$

the solution of the resulting closed-loop system is globally uniformly ultimately bounded.

The physical steering angle is obtained by inverse conversion of the virtual robust control law u_v .

$$\begin{aligned} \delta(y, \tilde{\theta}) = & \arctan \left(l \left[\frac{\cos^3 \tilde{\theta}_s}{(1 - yc(x))^2 \cos \hat{\alpha}_r} \left(\frac{dc(s)}{ds} y \tan \tilde{\theta}_s + u_v \right. \right. \right. \\ & \left. \left. \left. + c(s) (1 - yc(s)) \tan^2 \tilde{\theta}_s \right) + \frac{c(s) \cos \tilde{\theta}_s}{(1 - yc(s)) \cos \hat{\alpha}_r} \right] \right. \\ & \left. - \frac{l}{v \cos \hat{\alpha}_r} \frac{d \hat{\alpha}_r}{dt} + \tan \hat{\alpha}_r \right) - \hat{\delta}_b \end{aligned} \quad (62)$$

where $\tilde{\theta}_s = \tilde{\theta} + \hat{\alpha}_r$.

From the definition of a_2, a_3 in (49), it is proven that the lateral deviation y and the orientation error $\tilde{\theta}$ are globally uniformly ultimately bounded even in presence of both the inaccuracy

of the sliding angle reconstruction and the lateral disturbances. Meanwhile the closed-loop errors can be reduced by increasing the gains. In practice, to alleviate control chattering, the signum function $sign()$ is replaced by the hyperbolic tangent function $tanh()$

$$u_v = -Kz - \lambda_3 a_3 - \rho \tanh\left(\frac{\rho z}{\sigma}\right) \tag{63}$$

where σ is a positive constant determining the slope of the nonlinear switching curve.

Moreover, to tackle sustained disturbances which inevitably appear when a vehicle is following a circle or moving on a slope, a high-quality robust adaptive controller can be designed by using backstepping methods (Fang et al., 2006). The robust adaptive controller not only adapts to significant sustained non-linearity but also contains a robust term. Besides, the sliding mode fuzzy observer which is designed based on Takagi–Sugeno fuzzy model also provides an alternative robust solution against the sustained

disturbances (Oudghiri, Chadli, & El Hajjaji, 2007). The closed-loop stability can be achieved via averaging techniques.

5. Simulation results

5.1. Cornering stiffness identification

In order to validate the adaptive laws (40) for \hat{k}_f, \hat{k}_r with realistic simulations closely resembling actual experiments, a MATLAB-ADAMS co-simulation is carried out. The MATLAB/Simulink block diagram and ADAMS-Sub Module are shown by Figs. 3 and 4. In ADAMS a virtual vehicle with Fiala tire model is built and the tire-ground adhesion property is configured. Such a virtual test bed is employed to demonstrate the effectiveness of the proposed algorithms implemented in Matlab.

The parameters are set as $m=1500$ kg, $l_f=1.1$ m, $l_r=1.3$ m, $k_f=20\ 000$ N/rad, $k_r=25\ 000$ N/rad. The amplitude of the sine-like

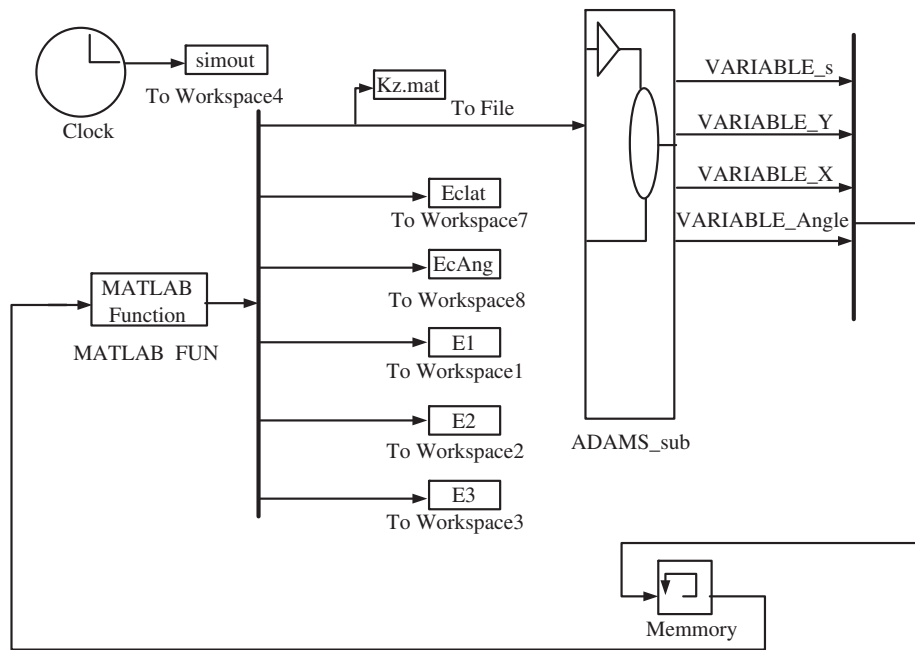


Fig. 3. MATLAB-Simulink block diagram of the closed-loop system.

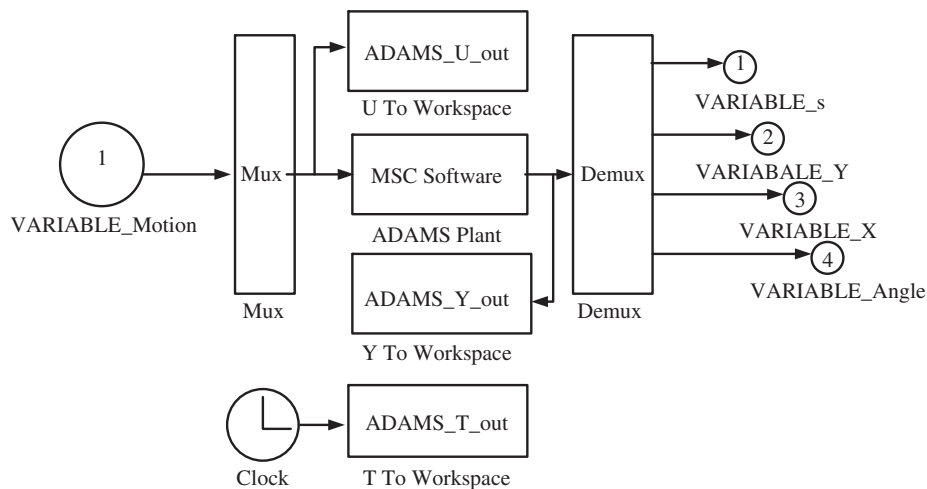


Fig. 4. ADAMS-Sub Module.

time-varying lateral disturbance which is the most common type of disturbances is set as $|\xi| = 1200$ N and $l_d = 0.8$ m. The vehicle velocity is set as a constant $v = 8.3$ km/h. In the simulations, the values of the cornering stiffness are initialized to zero, and the gains are set as $p_a = 500\,000$, $p_s = 2\,750\,000$, $k_1 = 20$, $k_2 = 3$, $\lambda_i = 10$. Random noise with zero mean and 0.8 variance is used as the steering input to excite the virtual vehicle system.

Both the classic Luenberger observer and the robust Luenberger observer are applied to identify the cornering stiffness. Comparative results of the identified \hat{k}_f, \hat{k}_r are shown by Fig. 5. From this figure it is seen that because the classic Luenberger observer has no ability to counteract the uncertain disturbances, the time-varying lateral disturbances lead to oscillating identification errors. While the robust Luenberger observer can provide satisfactory results, the identified values of \hat{k}_f, \hat{k}_r will converge into a neighborhood of the desired values obtained without disturbances, which is necessary for reconstructing the sideslip angles. The impact of the initial values on the identification results is also investigated. The initial values of the adaptive laws are set as 100, 10 000 and 35 000 N/rad, respectively. It is noticeable that all the identification results converge to their desired values with reasonable accuracy regardless of significant differences of the initial values (see Fig. 6).

The identification result of the cornering stiffness at the high speed $v = 13$ km/h is shown by Fig. 7. It demonstrates that the identification errors at the high speed are higher than that at the low speed when the time-varying disturbances are considered.

5.2. Simulation results of robust anti-sliding control

In this section, some simulation results of the robust anti-sliding control are presented. A reference path consisting of straight lines and curves is followed by the vehicles (see Fig. 8). Both the time-varying sine-like lateral disturbances and the side slip angles are introduced into the system. The Normal Lab Values of the side slip angles can be obtained by solving the dynamic equation (20). To compare with previous works, the control laws of Lenain et al. (2006a) as well as Thuilot et al. (2002) are also carried out.

Based on the identified \hat{k}_f, \hat{k}_r , the sideslip angle β is reconstructed without the knowledge of the lateral disturbances. The result is shown by Fig. 9 in which the desired value of β is

pseudo-measured by solving the dynamic equation (20). Since the cornering stiffness has been identified, the reconstruction of the sideslip angle may be obtained correspondingly. It is observed

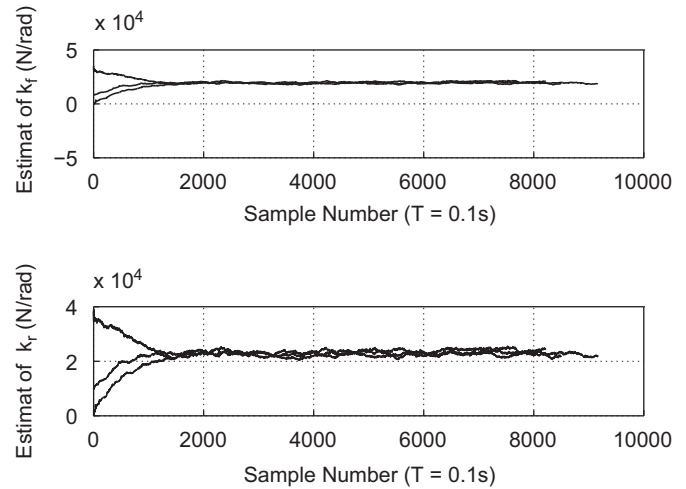


Fig. 6. Estimation of k_f, k_r at speed of 8.3 km/h.

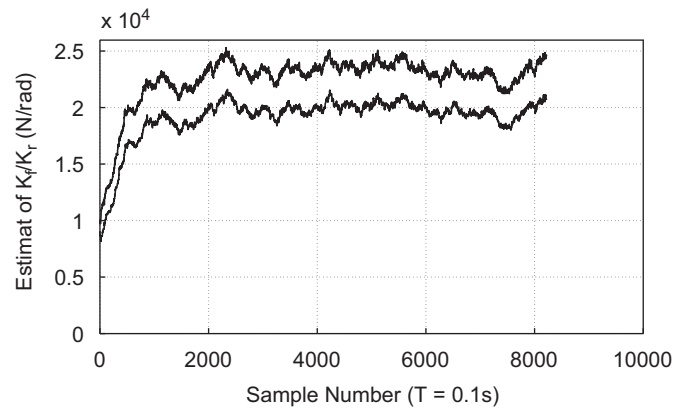


Fig. 7. Estimation of k_f, k_r at speed of 13 km/h.

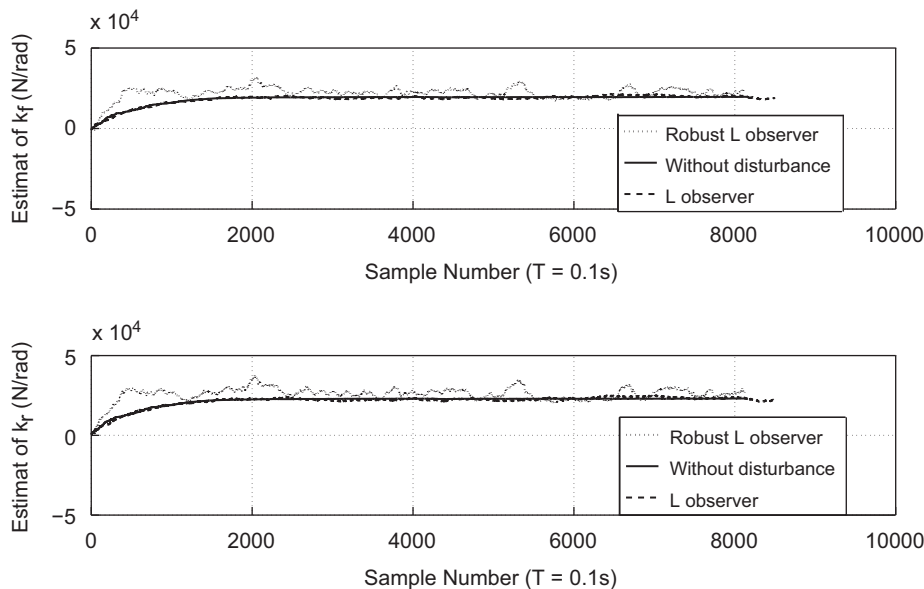


Fig. 5. Estimation of k_f, k_r at speed of 8.3 km/h.

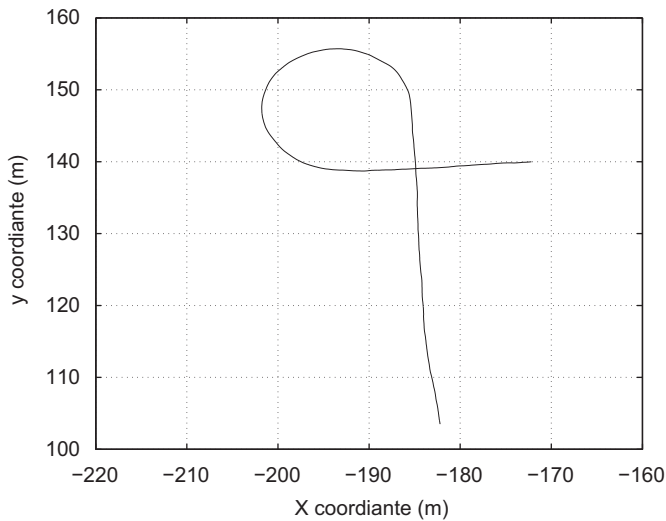


Fig. 8. Path to be followed.

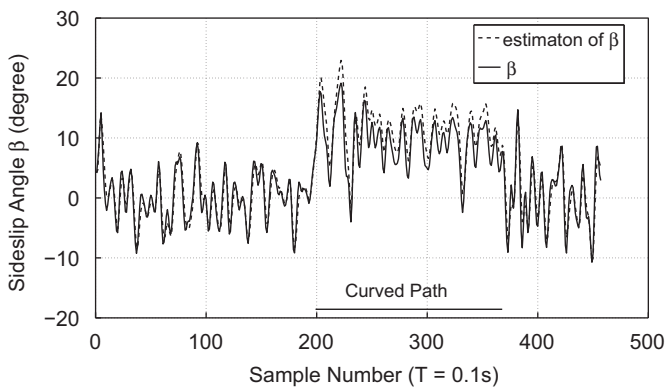


Fig. 9. Estimation of sideslip angle.

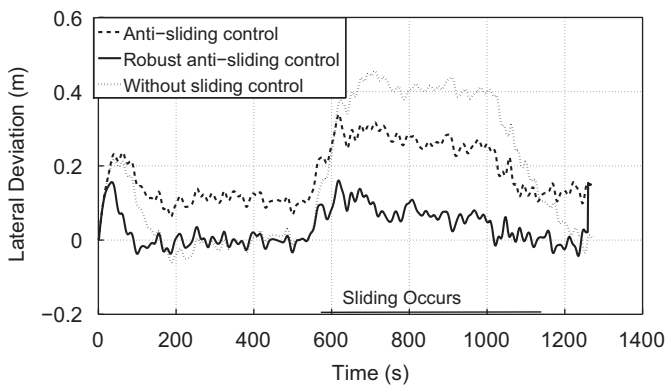


Fig. 10. Simulation results of lateral deviation.

that the sideslip angle becomes obviously prominent when the vehicle follows the curved path. Also a small amount of reconstruction errors are detected in Fig. 9. As explained in Section 3.2, the reconstruction errors are caused due to the negative effects of the time-varying lateral disturbance.

The simulation results of the lateral deviation are shown by Fig. 10. As the control law of Thuilot et al. (2002) does not take any sliding effects into account and the PD-type virtual control law is not robust against disturbances, it is clear that it will suffer from sliding significantly. When the sliding effects

appear, 40 cm lateral deviations are observed (dotted line). Although the anti-sliding controller of Lenain et al. (2006a) is effective to correct the negative sliding effects to some extent by compensating the sliding effects from kinematic point of view, it still cannot yield satisfactory results when the time-varying lateral disturbances are introduced into the system (dashed line). In contrast, the robust anti-sliding controller proposed in this paper can stabilize the system states and provide satisfactory simulation results with 10 cm lateral accuracy. It has good transient responses and is robust against not only the sliding effects but also the time-varying disturbance (solid line).

6. Experimental results

The proposed robust Luenberger observer and sliding compensation controller have been implemented and successfully tested on an autonomous vehicle—(500CC RTV Utility Vehicle) shown by Fig. 11. The rotating velocity of the rear wheel was measured by optical rotary encoders. The actual steering angle of the front wheel was measured by means of absolute encoders and compared with its desired value. A PD algorithm implemented on a micro-processor controlled the electro-hydraulic valve of the steering mechanical system. The measurement of the yaw rate was obtained by using Crossbow VG700CB FIBER OPTIC VERTICAL GYRO with 0.75° accuracy and the side-acceleration is also measured by ADXL202 at the mass center with 2 mg resolution. The GPS is dual frequency EPOCH 25 RTK GPS with ± 10 mm accuracy and 10 Hz sampling frequency.

Too small values of the forward velocity make it difficult to maintain stability and controllability of the wheeled vehicles due to nonholonomic kinematic constraints when the control inputs are constrained. But the upper bound of the velocity is also limited when the inner closed-loop delays of the electro-hydraulic steering system have to be taken into account. So the range of the allowable velocity of the test bed is 3–15 km/h. Furthermore, if the vehicle is driven at high speeds, then dynamics-based control methods and nonlinear tire models become necessary.

The efficiency of the algorithm to identify the cornering stiffness has been tested. The vehicle was maneuvered by a human driver in an arbitrary fashion on the slippery grassplot and dry roads with the velocity $v=8.3$ km/h. The lateral disturbances with significant magnitudes were encountered due to sudden changes of the bank angles and bumps of the roads. Since the adherence properties of certain kinds of ground do not vary greatly, the proposed adaptive laws can yield the corresponding identification results of k_f, k_r . More importantly, even when the ground properties change significantly from the slippery grassplot



Fig. 11. RTV Utility Vehicle.

to the dry roads, the proposed adaptive laws for \hat{k}_f, \hat{k}_r can still work well to trace the varying of the cornering stiffness in robust manner against the lateral disturbances (Fig. 12). Although the underlying cornering stiffness is not exactly known, the results of this identification experiment are satisfactory.

As a physical quantity, the cornering stiffness which is only relevant to tire-ground contact characteristics does not vary greatly. However, the applicability of the proposed adaptive identification law depends on a proper model representation of the complex reality. Since the cornering stiffness is used as a tuning factor, the variations of the identified cornering stiffness as shown in Fig. 12 are mainly due to inherent difficulties in the mathematical modeling of the parameter uncertainties and unknown disturbances. The reconstructed sideslip angle β on the slippery and dry roads is shown in Figs. 13 and 14, respectively. In both cases, sliding occurs inevitably, but the sideslip angle on the slippery road changes with large magnitude. Meanwhile the slip angle on the dry road changes more violently but with small magnitude. This is due to the fact that the large cornering stiffness k_r, k_f can provide large tire forces which can correct the tire-sliding more powerfully.

It should be noted that the whole experimental process consists of two stages. In the first stage the cornering stiffness is identified. In the second stage, based on the identification results, the robust anti-sliding controller is used to improve the accuracy of the path following control. The framework of this two-stage scheme is quite applicable in practice when the tire-ground adhesion property is evenly distributed approximately and leads to stable and effective behaviors of the whole auto-steering control system. For a certain type of ground, when the variance of the averaged identification results is less than a defined

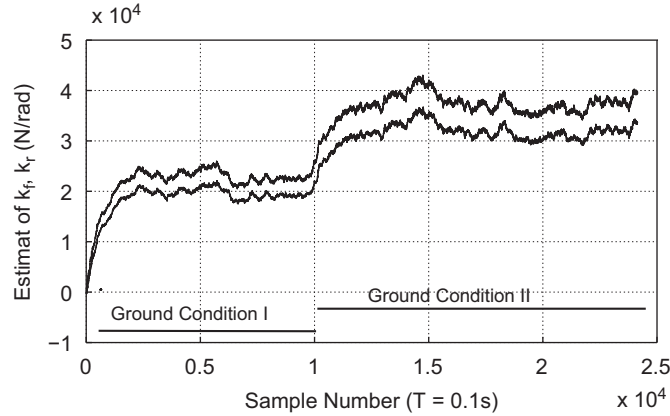


Fig. 12. Estimation of cornering stiffness.

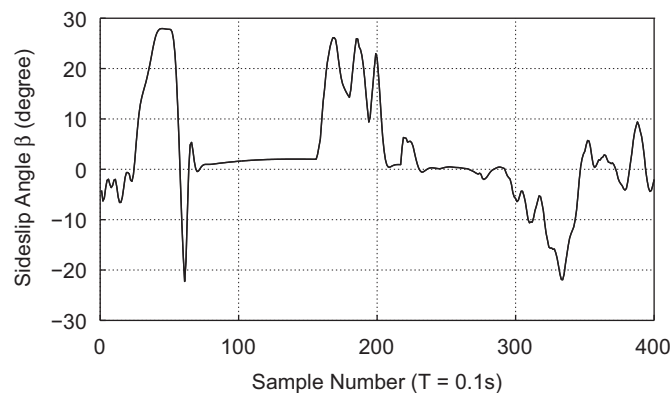


Fig. 13. Estimation of sideslip angle on slippery ground.

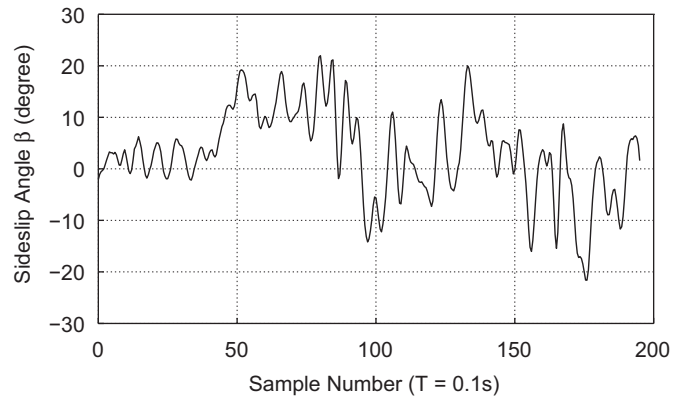


Fig. 14. Estimation of sideslip angle on dry roads.

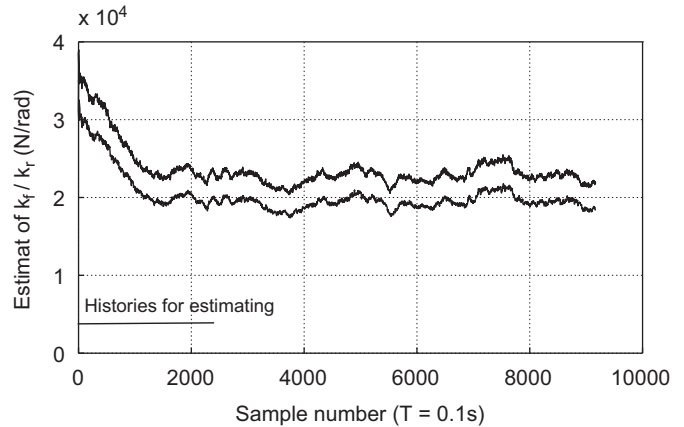


Fig. 15. History for using estimated cornering stiffness.

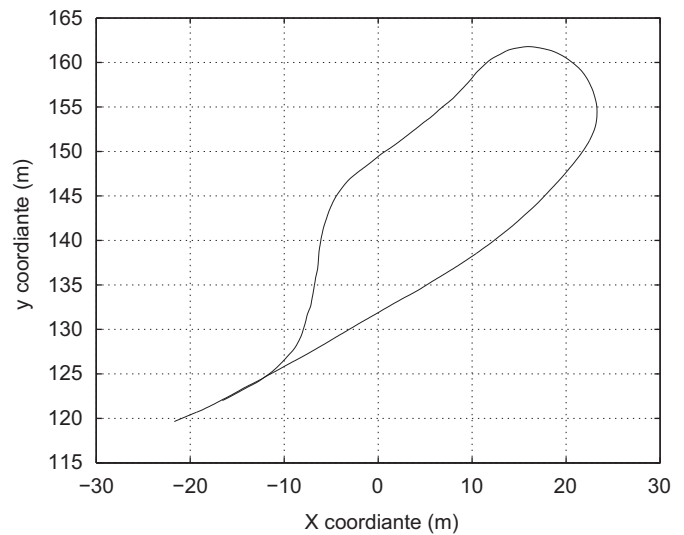


Fig. 16. Path to be followed.

threshold (see Fig. 15), which means that the identified cornering stiffness has converged to a reasonable value, the vehicle is automatically steered to follow the reference path. Even if the ground adhesion condition varies gradually which would prolong the transient period for the parameter identification, the stability of the lateral control still can be guaranteed with the help of the robust anti-sliding controller (62).

In real-world applications a reference path consisting of straight lines and curves (Fig. 16) was followed. First, the control

law of Thuilot et al. (2002) was tested. The lateral deviation is shown by dashed line in Fig. 17. It is shown that the controller of Thuilot et al. (2002) can provide satisfactory results when the vehicle follows the straight parts of the reference path, and the lateral deviation oscillates within the range of 10 cm. But when the vehicle starts to follow the curves, due to low-grip conditions of the slippery grounds, the tire adherence cannot provide enough lateral forces for the vehicle to track the curve, the tire sliding angles obviously increase (Fig. 18), resulting in significant lateral deviations (Dashed line in Fig. 17). Based on the identification of k_f, k_r , the front/rear sliding angle is reconstructed on line (Fig. 18). In Fig. 18 a large rear sliding angle caused by initial adjustment of the vehicle's body attitude is recorded at the beginning of the test. The sliding angles vary around zero, which means that no obvious sliding occurs. But when the vehicle begins to follow the curve, the magnitude of the sliding angles increases to 5–10 degree, which indicates that the tire sliding occurs obviously. And it is also observed that the slip angle of the front wheel is larger than that of the rear wheel especially when sliding occurs. This is caused by rapid steering maneuver, i.e. understeer situation.

Relying on the reconstruction of the sliding angles and the proposed robust anti-sliding controller, not only the sliding effects but also the lateral disturbances are neutralized. When the vehicle begins to follow the curve, although low-level delay may lead to obvious errors at the beginning and end of the curve tracing, the robust anti-sliding controller can compensate the tire-sliding angles and make the vehicle motion robust against the inaccuracy of the sliding angle reconstruction and the lateral disturbances (Solid line in Fig. 17). The orientation errors are displayed in Fig. 19. The controller may improve the orientation control accuracy, but as analyzed in Section 4, the orientation

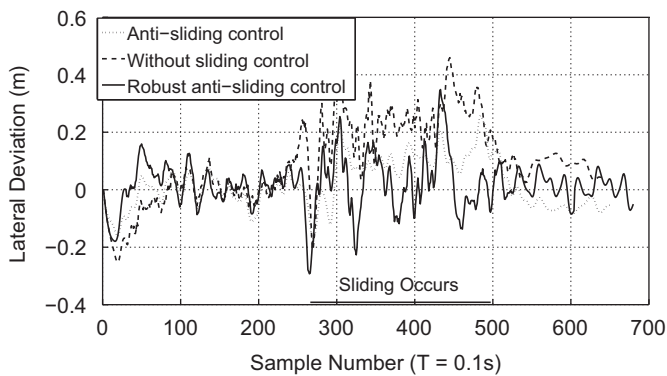


Fig. 17. Lateral deviation of experimental results.

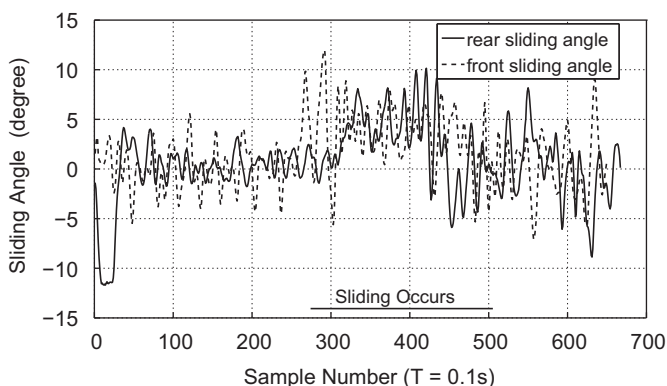


Fig. 18. Sliding angle estimation without sliding compensation.

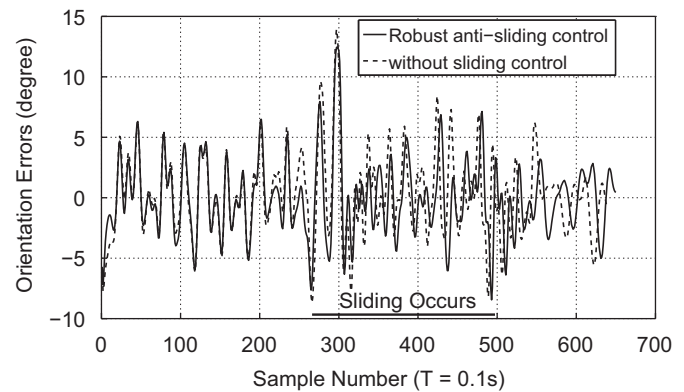


Fig. 19. Orientation error of experimental results.

errors cannot be totally eliminated. It fits very well with the performance of the vehicle in actual experiments.

The MSE (Mean Squared Error) of CWSC (Controller Without Sliding Control) is 0.2684, ME (Mean error) is 0.1907. The results of the anti-sliding controller of Lenain et al. (2006a) using the kinematic observer are also shown in Fig. 17 (dotted line). The MSE of ASC (Anti-Sliding Control) is 0.1084, and ME is 0.0657. The MSE of RAC (Robust Anti-Sliding Control) is 0.1263, and ME is 0.0464. It is quite interesting to see the different performances of those two kinds of the controllers. The robust controller can provide satisfactory lateral accuracy at the expense of high-gain and un-smooth control. Consequently, it can yield small mean errors w.r.t. the reference path, but the vehicle motion may be too drastic. In contrast, the anti-sliding controller of Lenain et al. (2006a) leads to relatively smooth vehicle motion without too much vibration, but its lateral deviation is much greater than that of the RAC.

7. Conclusion

This paper developed and investigated a robust algorithm for cornering stiffness identification. Based on the measurements of the side-acceleration and yaw rate, the cornering stiffness was identified by using a robust adaptive Luenberger observer in presence of time-varying lateral disturbances. The stability of the observer was proven via Lyapunov analysis. The sideslip angle was reconstructed based on the lateral dynamic equations and the identified tire cornering stiffness. Since the time-varying lateral disturbance may degrade the effective performance of the sliding angle reconstruction, a robust path-following controller which was robust to both the inaccuracy of the sliding angle reconstruction and the lateral disturbances was designed based on the chained system theory. The proposed control scheme has important applications in improving maneuverability of Rough Terrain Vehicles (RTV). In future works, adaptive robust observers and controllers which do not rely on the assumption of constant velocity and cornering stiffness are to be designed in more general ways.

References

- Abe, M. (1992). *Vehicle Dynamics and Control*. Sankaidou Publication (in Japanese).
- Ackermann, J. (1997). Robust control prevents car skidding. *IEEE Control Systems Magazine*, 17(3), 23–31.
- Baffet, G., Charara, A., & Lechner, D. (2009). Estimation of vehicle sideslip, tire force and wheel cornering stiffness. *Control Engineering Practice*, 17(11), 1255–1264.
- Bevly, D. M. (2004). Global positioning system (GPS) a low-cost velocity sensor for correcting inertial sensor error on ground vehicles. *Journal of Dynamic Systems, Measurement, and Control*, 126(2), 255–265.

- Bevly, D. M., Gerdes, J. C., Wilson, C., & Zhang, G. (2000). The use of GPS based velocity measurement for improved vehicle state estimation. In *IEEE proceeding of the American control conference* (Vol. 4, pp. 2538–2542). Chicago, IL.
- Bevly, D. M., Sheridan, R., & Gerdes, J. C. (2000). Integrating INS sensors with GPS velocity measurements for continuous estimation of vehicle sideslip and tyre cornering stiffness. In *IEEE proceeding of the American control conference* (Vol. 4, pp. 25–30). Chicago, IL.
- Corradini, M. L., & Orlando, G. (2002). Experimental testing of a discrete-time sliding mode controller for trajectory tracking of a wheeled mobile robot in the presence of skidding effects. *Journal of Robotic Systems*, 19(4), 177–188.
- D'Andrea-Novet, B., Campion, G., & Bastin, G. (1995). Control of wheeled mobile robots not satisfying ideal constraints: a singular perturbation approach. *International Journal of Robust Nonlinear Control*, 16(5), 243–267.
- Fang, H., Lenain, R., Thuilot, B., & Martinet, P. (2004). Sliding mode control of automatic guidance of farm vehicles in the presence of sliding. In *The 4th international symposium on robotics and automation* (pp. 582–587). Queretaro, Mexico, August 25–27.
- Fang, H., Lenain, R., Thuilot, B., & Martinet, P. (2005a). Robust adaptive control of automatic guidance of farm vehicles in the presence of sliding. In *IEEE international conference on robotics and automation* (pp. 3113–3118). Barcelona, April 18–22.
- Fang, H., Lenain, R., Thuilot, B., & Martinet, P. (2005b). Trajectory tracking control of farm vehicles in presence of sliding. In *IEEE/RSJ international conference on intelligent robots and systems*. Alberta, August 2–6.
- Fang, H., Fan, R. X., Thuilot, B., & Martinet, P. (2006). Trajectory tracking control of farm vehicles in presence of sliding. *Robotics and Autonomous Systems*, 54(10), 828–839.
- Hahn, J.-O., Rajamani, R., & Alexander, L. (2002). GPS-based real-time identification of TireC/Road friction coefficient. *IEEE Transactions on Control Systems Technology*, 10(3), 331–343.
- Hiraoka, T., Kumamoto, H., & Nishihara, O. (2004). Sideslip angle estimation and active front steering system based on lateral acceleration data at centers of percussion with respect to front/rear wheels. *JSAE Review*, 25(1), 37–42.
- Hiraoka, T., Kumamoto, H., Nishihara, O., & Tenmoku, K. (2001). Cooperative steering system based on vehicle sideslip angle estimation from side acceleration data at percussion centers. In *Proceedings of IEEE international vehicle electronics conference (IVEC2001)* (pp. 79–84).
- Jiang, Z. P., & Hill, D. J. (1999). A robust adaptive backstepping scheme for nonlinear systems with unmodeled dynamics. *IEEE Transactions on Automatic Control*, 44(9), 1705–1711.
- Lenain, R., Thuilot, B., Cariou, C., & Martinet, P. (2006a). Sideslip angles observer for vehicle guidance in sliding conditions: Application to agricultural path tracking tasks. In *Proceedings of the international conference on robotics and automation* (pp. 3183–3188). Florida: Orlando, May.
- Lenain, R., Thuilot, B., Cariou, C., & Martinet, P. (2006b). Mobile robot control in presence of sliding: Application to agricultural vehicle path tracking. In *Proceedings of the 45th IEEE conference on decision & control* (pp. 6004–6009). CA, USA: San Diego, December 13–15.
- Leroquais, W., & D'Andrea-Novet, B. (1997). Vibrational control of wheeled mobile robots not satisfying ideal velocity constraints: The unicycle case. In *European Control Conference*. Brussels, July 1–4.
- Low, C. B., & Wang, D. (2007). Integrated estimation for wheeled mobile robot posture, velocities, and wheel skidding perturbations. In *IEEE international conference on robotics and automation* (pp. 2355–2360). Italy: Roma, April 2007.
- Low, B. C., & Wang, D. (2008). GPS-based path following control for a car-like wheeled mobile robot with skidding and slipping. *IEEE Transactions on Control Systems Technology*, 16(2), 340–347.
- Motte, I., & Campion, H. (2000). Control of sliding mobile robots: A slow manifold approach. In *Fourth symposium on mathematical theory of networks and systems (MTNS 2000)*. France: Perpignan.
- Oudghiri, M., Chadli, M., & El Hajjaji, A. (2007). Lateral vehicle velocity estimation using fuzzy sliding mode observer. In *Proceedings of the 15th mediterranean conference on control & automation*. Greece: Athens, July 27–29.
- Samson, C. (1995). Control of chained systems. Application to path following and time varying point stabilization of mobile robot. *IEEE Transactions on Automatic Control*, 39(12), 2411–2425.
- Sierra, C., Tseng, E., Jain, A., & Peng, H. (2006). Cornering stiffness estimation based on vehicle lateral dynamics. *Vehicle System Dynamics*, 44(1), 24–38.
- Stephant, J., Charara, A., & Meizel, D. (2004). Virtual sensor, application to vehicle sideslip angle and transversal forces. *IEEE Transactions on Industrial Electronics*, 51(2), 278–289.
- Thuilot, B., Cariou, C., Martinet, P., & Berducot, M. (2002). Automatic guidance of a farm tractor relying on a single CP-DGPS. *Autonomous Robots*, 13(1), 87–104.
- Wang, D., & Low, C.B. (2007). An analysis of wheeled mobile robots in the presence of skidding and slipping: Control design perspective. In *IEEE international conference on robotics and automation* (pp. 2379–2384). Italy: Roma, April 2007.
- Zhang, Y. L., Chung, J. H., & Velinsky, S. A. (2003). Variable structure control of a differentially steered wheeled mobile robot. *Journal of Intelligent and Robotic Systems*, 36(3), 301–314.